Characterization of mixture preparation in a direct-injection internal combustion engine fueled with hydrogen using PIV and PLIF

Victor M. Salazar[1], Sebastian A. Kaiser[2]

1: Combustion Research Facility, Sandia National Laboratories Livermore, CA, USA, vmsalaz@sandia.gov
2: Combustion Research Facility, Sandia National Laboratories Livermore, CA, USA, sakaise@sandia.gov

Abstract This paper examines the in-cylinder flow and mixing during the compression stroke of a direct-injection hydrogen-fueled internal combustion engine. The velocity in the vertical symmetry plane of the cylinder of an optically accessible engine was measured by particle image velocimetry (PIV) and, separately, the hydrogen mole-fraction by planar laser-induced fluorescence (PLIF) of acetone as a fuel tracer. Two intake configurations of the four-valve engine head were used: In the standard configuration, there is little coherent charge motion, while a modified version produces strong tumble flow. This tumble flow is counter-acting the large-scale rotational charge motion caused by the wall jet that forms after injection from the angled, centrally located single-hole nozzle. The injection momentum dominates the in-cylinder flow, but with higher intake-induced momentum, the circumferential convection is modified and slowed, such that the fuel distribution towards the end of the compression stroke is significantly different from that for low intake-induced tumble. For the low-tumble case, the root-mean-square (RMS) fields of velocity and scalar are examined. They indicate that the fuel jet upstream of impingement has similar turbulence structure as canonical fully developed turbulent jets. Neither in that unimpinged part of the jet nor in the wall jet are regions of maximum velocity RMS collocated with regions of maximum scalar RMS. In single-shot images, regions of high hydrogen mole-fraction at the edge of the wall jet's head are often at an angle of about 45 degrees with respect to the mean flow, a feature also found in steady free jets.

1. Introduction

Hydrogen, with its excellent properties as fuel (Karim 2003) has shown promising benefits for applications in internal combustion engines and fuel cells. So far, fuel cells offer the best well-to-wheels efficiency and emissions (Edwards et al. 2004). However, due to their high cost and the lack of a hydrogen-refueling infrastructure, many experts believe that their deployment to the market is at least 10-20 years away (Edwards et al. 2004, Rousseau et al. 2008, Delorme et al. 2009). Conversely, hydrogen-fueled internal combustion engines (H2ICEs) can take advantage of the current engine-manufacturing infrastructure to be mass-produced cost-effectively. Additionally, recent system studies show that advanced H2ICE-powered vehicles can outperform gasoline vehicles and are very competitive with fuel cells (Delorme et al. 2009). For these reasons, hydrogen engines are seen as a bridging technology that will help to accelerate the development of hydrogen-based infrastructure.

Advanced hydrogen-engine concepts are based on direct-injection (DI) fuel systems. In contrast to port-injection, DI not only avoids loss of power due to low volumetric efficiency, but also can mitigate combustion problems such as knock, backfire, and pre-ignition, which have detrimental effects on engine performance and emissions (White et al. 2006). DI can also reduce heat transfer losses, which in hydrogen engines, due to the low flame quenching distance, are relatively high. Studies on DI-H2ICEs (Wallner et al. 2008, Salazar and Kaiser 2009) show that the extent of benefit from DI depends in great degree on the injection strategy and the subsequent mixture formation. Therefore, understanding the details of injection and mixing is an imperative step to improve the efficiency of future hydrogen engines. Our previous optical measurements (Salazar and Kaiser 2009) suggest that jet-wall interactions dominate the mixing process. However, the role

of intake-induced charge motion in mixture formation is unclear, mainly because its effect is superimposed onto the momentum from the fuel jet. Tumble, conventionally defined as rotational motion of the in-cylinder flow perpendicular to the cylinder axis, has significant effects on mixture formation and engine performance in gasoline engines (Hill and Zhang 1994). It is believed that the large-scale tumble vortex generated during intake initially strengthens during compression but then breaks down near top dead center (TDC). This breakdown transfers the kinetic energy stored at the integral scale to the smaller scales of turbulence, increasing turbulence intensity at TDC and consequently the flame speed (Boree et al. 2002, Moreau et al. 2004).

In DI H2ICEs, due to the wide flammability limits of hydrogen, the load can be controlled by the amount of fuel injected into the cylinder. At high loads (richer mixture), the flame propagates very fast, however at low loads (leaner condition) the flame speed decreases (Bradley et al. 2007, Knop et al. 2008) to the point where combustion duration is too long for optimal efficiency. This is somewhat contrary to the generally maintained notion that "hydrogen burns very fast". That is certainly true at stoichiometric conditions. However, while hydrocarbon-fueled engines have to operate relatively close to stoichiometric, it is possible to run H2ICEs lean enough to reach idling conditions unthrottled. Homogenous low-load operation is not desirable due to high cycle-to-cycle variability and long combustion duration. It is then important to understand how the charge motion influences the final state of stratified fuel-air mixtures in a hydrogen engine at low loads.

As in commercial diesel engines, hydrogen injectors for production vehicles will most likely have multi-hole nozzles to aid rapid fuel/air mixing. However, to gain a fundamental understanding of the physical processes involved in mixture preparation and as a bench mark for initial simulation validation, single-hole injectors have proven very valuable (Salazar and Kaiser 2009, Wallner et al. 2009). In the current study, an angled single-hole nozzle allowed adding momentum to the in-cylinder flow (Salazar and Kaiser 2010). The interaction of the injection event with the intake-induced charge motion was studied using separate, two-dimensional measurements of the velocity and scalar fields by particle image velocimetry (PIV) and planar laser-induced fluorescence (PLIF), respectively. To track the evolution of fuel/bulk-gas mixing, measurements from bottom dead center (BDC) to near top dead center (TDC)[1] were performed for two intake configurations with different amounts of intake-induced charge motion. Besides understanding the physical processes in mixture formation, the objective of this study is to add to a broad database that can be used to validate numerical simulations.

2. Experiment and Data Reduction

2.1. Optical engine and hydrogen injector

Experiments were performed using a passenger-car sized, optically accessible, single-cylinder engine adapted to operate with hydrogen. Schematics of the relevant optical and mechanical components are shown in Figure 1. The engine uses a four-valve four-stroke single-cylinder GM research head with a pent-roof combustion chamber. The piston is flat-topped. The intake system consists of two intake ports, one for each valve, both straight and parallel to each other, forming an angle of 40° with respect to the fire deck (horizontal). For this study, a full-length fused-silica liner was used such that the entire volume swept by the cylinder was optically accessible. Some engine parameters are given in Table 1.

[1] The crank-angle convention used here assigns 0ºCA to compression TDC, i.e., crank angles throughout the compression stroke are negative.

Table 1 Engine Specifications

Bore	92 mm
Stroke	85 mm
Displacement	565 cm^3
Compression ratio	11
Speed	1500 rpm
Intake pressure / Temperature	1 bar / 36°C
Intake valve timing	open: 346°CA / close: -140°CA
Exhaust valve timing	open: 130°CA / close: -356°CA
Injection timing	start: -137°CA / end: -120.5°CA

Hydrogen was supplied at 100 bar directly into the combustion chamber via a solenoid injector from Westport Inc. As shown in Figure 1a, the injector nozzle has a single hole with a diameter of 1.46 mm at a 50° angle with respect to the injector axis. Figure 1b shows the injector location, centrally located between the four valves, and the nozzle direction, aiming towards the intake between the two valves and downward. Hence the jet was aligned with the mirror-symmetry plane of the combustion chamber. All measurements reported here were taken in this central symmetry plane.

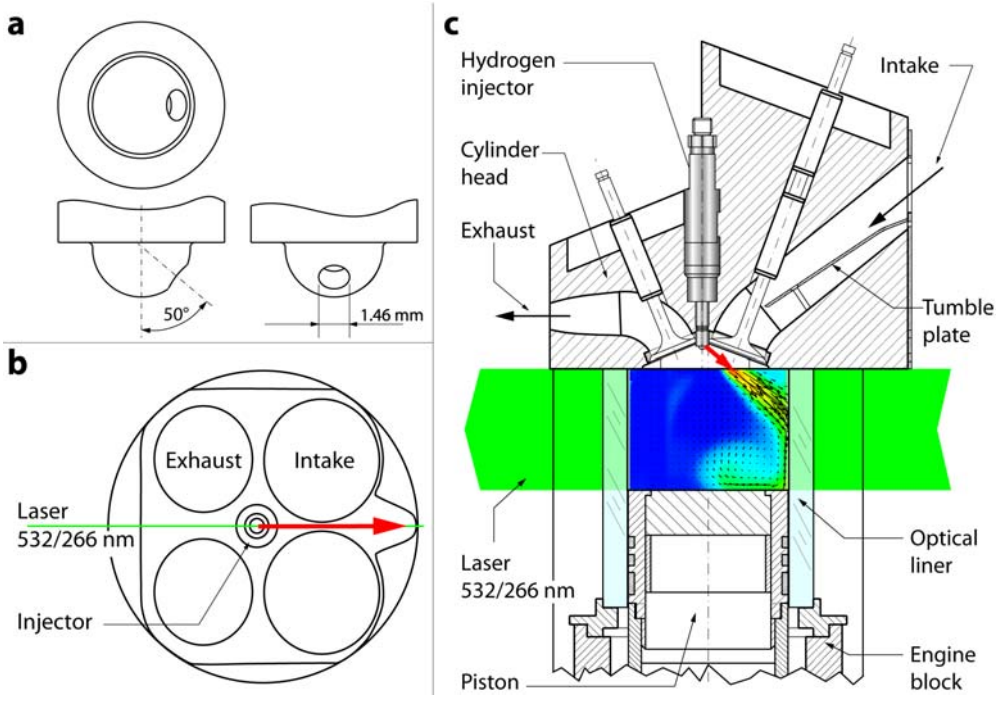

Figure 1 Schematics of engine hardware. (a) Geometry of the single-hole injector nozzle, (b) location and targeting of injector with respect to the combustion chamber, (c) upper engine with measurement plane.

2.2. Velocity measurements

PIV is a mature laser-diagnostic technique widely used for flow-field measurements. In engines, it has been successfully applied to evaluate both the in cylinder and intake flow fields (Boree et al. 2002, Li et al. 2002, Miles et al. 2007, Muller et al. 2010).

In the present work, silicon dioxide (SiO_2) particles with a nominal diameter of 2.3 μm were seeded into the intake flow by a modified TSI particle seeder (Model 3400A). These particles were sufficiently small to follow the large-scale motions of the flow that are of interest here. The beams from a dual-head Nd:YAG laser operating at 532 nm with an energy of about 2 x 60 mJ/pulse were formed into overlapping vertical light sheets, directed into the cylinder through the optical liner as shown in Figure 1c. The particle-scattered light was imaged by a dual-frame CCD camera. The field of view covered the full bore and stroke, but not the pent-roof, which cannot be illuminated from the side with the current arrangement. The imaged region extends to within less than a millimeter of the walls and piston top. The time delay between laser pulses was optimized for each measurement, resulting in delays ranging from 0.8 μs during the injection event to 20 μs late in the compression stroke.

Vector evaluation was performed using LaVision's DaVis 7.0 software. First, the images were corrected for distortion induced by the curved optical liner. Subsequently, vectors fields were computed using a multi pass cross correlation technique (Keane and Adrian 1992, Keane et al. 1995) with final interrogation areas of 32 x 32 pixels^2 and 50% overlap. This corresponds to a spatial resolution of 2.95 x 2.95 mm^2. The vectors were then validated using a local median filter (Westerweel 1994). Areas where strong reflections from the optical liner overwhelmed the actual particle scattering were exempt from vector evaluation by appropriate masks. Missing vectors were not filled in by interpolation. Typically, about 175 images were collected phase-locked at each crank-angle. The crank angles examined here range from BDC to -30°CA.

2.3. Scalar measurements

Imaging of the hydrogen mole-fraction was performed in the same region and at the same crank angles as PIV, but in separate measurements. Planar laser-induced fluorescence (PLIF) of gaseous acetone as a fuel tracer was adapted to obtain quantitative images of the hydrogen mole-fraction in the operating engine. The imaging technique is described in detail in previous work (Salazar et al. 2009) and is therefore discussed only briefly here. Acetone was seeded as a tracer into the hydrogen fuel by a high-pressure bubbler. At 100 bar and room temperature, a volume concentration of 0.33% can be reached. For current purposes, differential diffusion of tracer and fuel is estimated to be insignificant due to the large spatial structures examined here and the high Reynolds number of the post-injection flow. A quadrupled Nd:YAG at 266 nm laser excited acetone fluorescence. Laser energies of about 100 mJ/pulse and a sheet-forming lens combination with f = 1500 mm were used. An f = 50 mm, *f*/1.2 camera lens with an achromatic f = 500 mm "close-up" lens focused the visible part of the acetone fluorescence onto an unintensified, back-illuminated CCD camera. Rejection of elastically scattered UV laser-light by the glass lenses was sufficiently good to omit a long-pass filter. The imaged region was slightly less than for PIV, extending to about a millimeter from the cylinder walls.

Standard background and flat-field corrections are performed to quantify the measurements. For the latter, a nearly homogeneous charge was prepared by DI during the intake stroke. As in the PIV measurements, distortion due to the curved liner needed to be corrected. Inhomogeneities in the temperature field, induced by mixing of cold hydrogen and hot bulk gas, were corrected for based on known spectroscopic properties of the tracer (Thurber et al. 1998, Thurber and Hanson 1999) and the assumption of adiabatic mixing between fuel and bulk gas (Yeh et al. 1994, Espey et al. 1997, Hwang et al. 2007, Salazar et al. 2009). This correction also yields an approximate temperature field. The overall typical maximum error in the ensemble-mean mole-fraction fields is

estimated to be 25%. Small regions, in particular for early crank angles, may have larger errors because window fouling and signal reflections can be locally severe for this imaging configuration. 90 images of hydrogen mole-fraction were collected at each crank-angle.

2.4. Tumble ratio

The tumble ratio TR, defined as the ratio of the equivalent solid-body angular speed to the engine speed, was calculated from the mean velocity distribution by Equation 1.

$$TR = \frac{\sum_{i=1}^{n}\sum_{j=1}^{m} \rho_{i,j}(\vec{r}_{i,j} - \vec{r}_c) \times \vec{V}_{i,j}}{\omega . \sum_{i=1}^{n}\sum_{j=1}^{m} \rho_{i,j}(\vec{r}_{i,j} - \vec{r}_c) \bullet (\vec{r}_{i,j} - \vec{r}_c)} \qquad (1)$$

where $\vec{r}_{i,j} - \vec{r}_c$ is the distance of a given location with indices *(i,j)* to the center of rotation, $\vec{V}_{i,j}$ and $\rho_{i,j}$ the velocity and density, respectively, in that location, and ω the engine's angular (crank shaft) speed. The local density ρ was calculated from the mean hydrogen mole-fraction and temperature fields. In the present work, we chose as the center of rotation the centroid of the cylinder symmetry-plane, including the pent-roof, which is not imaged by the PIV measurements. The center of rotation thus moves upwards as the piston reduces the chamber volume towards TDC. Since it is based on two-dimensional measurements in a single plane, the TR reported here is not that of the entire charge in the cylinder, but only describes the charge motion in that plane.

2.5. Experimental conditions

Because the present study is focused on the mixture-preparation process prior to ignition, fired operation was not necessary. The engine was motored at a constant speed of 1500 rpm, and nitrogen was supplied as a bulk gas (but treated as air in calculations of the equivalence ratio). The pressure in the surge tank upstream of the intake runner was kept at 1 bar and typical intake temperatures just upstream of the engine head were around 36°C.

To obtain a global equivalence ratio of 0.25 ($\lambda = 4.0$) or a hydrogen mole-fraction of 0.095, the hydrogen fuel was injected for 17.5°CA at 100 bar. In fired operation at typical efficiencies, this fuel concentration represents a low-load condition with about 2.5 bar IMEP. The fuel injection started shortly after intake-valve closure to yield the maximum time span for observable interaction with the intake-induced flow. With the injection command issued at -140°CA, flow from the nozzle started at -137°CA and ended at -120.5°CA.

Due to the injection direction the angular momentum of the hydrogen jet is counter-acting that of the intake flow. As part of this study, the intake geometry was modified to induce stronger intake tumble, and the effects of this modified flow on the charge motion after injection were observed. There are several ways to increase the tumble ratio in an engine (Hill and Zhang 1994, Arcoumanis et al. 1998, He et al. 2007). Here, we inserted tongue-like plates into the intake ports, gradually reducing the cross-section of each port to its upper half, thereby directing the intake flow more along the pent-roof than would be the case without modifications. The engine head with tumble plates is shown in Figure 1c. In the following, when comparing operation with the unmodified head to that with tumble plates inserted, the former will be described as "low tumble" and the latter as "high tumble" operation.

3. Results and Discussion

3.1. Mean scalar and velocity fields

Since PLIF and PIV measurements were performed separately, the instantaneous correlation between hydrogen mole-fraction and velocity cannot be determined. However, the mean scalar and velocity fields, shown in Figure 2, give a good overview of the mixture-formation throughout the compression stroke.

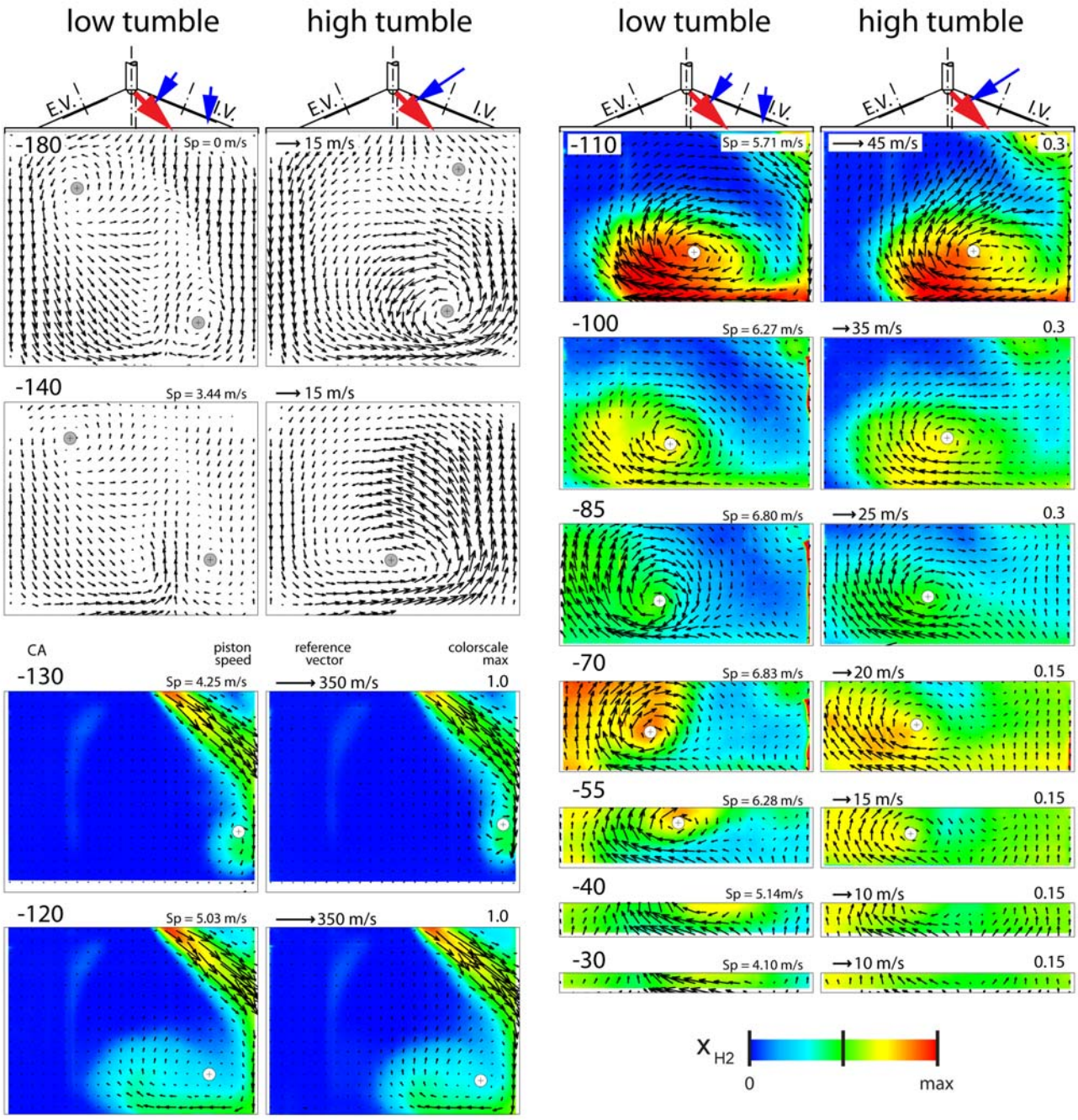

Figure 2 Mean velocity (arrows) and mean hydrogen mole-fraction (background color) for low and high tumble. The engine head with direction of injection and intake flow is shown schematically above each column. Above each image pair (left to right): Crank angle, piston speed S_p, reference vector length, and peak of color scale for the mole fraction. For clarity, only every third velocity vector is plotted. The center of prominent vortices is marked by a white circle.

At BDC (-180°CA), the mean velocity fields indicate that for the low-tumble configuration there is not a single, well-defined tumble vortex. Instead, two counter-rotating vortices are observed: one with its center at the top left and another one at the bottom right. The flow structure observed here is generated by a combination of wake recirculation under the partly open valves and flow redirection by cylinder liner and piston top. This pattern can also be clearly seen in the classic results of Khalighi (Khalighi 1990). With the tumble plates inserted, on the other hand, a strong, well-defined tumble vortex is observed near the piston top, accompanied by a much weaker secondary one below the intake valves. The TR, shown in Figure 3, is four times greater for the high-tumble case than for low tumble. Just before injection, at -140°CA, velocities for low tumble have decreased further, but have remained at the previous level for high tumble. There is still a factor of four in TR between the two cases.

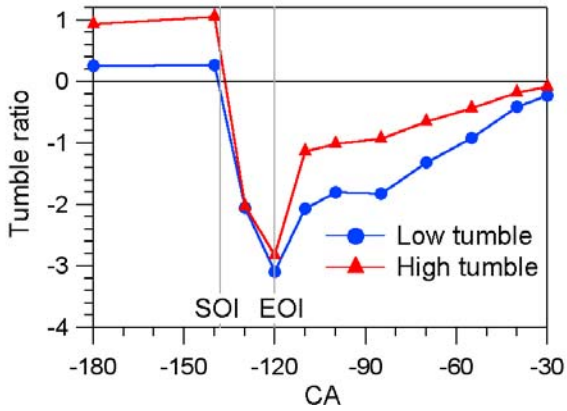

Figure 3 Tumble ratio with injection into low and high-tumble in-cylinder flow.

At -130°CA, 7°CA or 0.78 ms after the jet start, the fuel has impinged on the cylinder wall forming a wall-jet recirculation vortex. Typical centerline velocities within the free jet are measured to be about 300 m/s, more than one order of magnitude higher than typical velocities in the undisturbed flow field. Correspondingly, the TRs have been reversed in sign and increased in magnitude. While the free-jet velocities do not differ significantly between the two cases, the wall jet is already starting to show subtle influence of the intake-induced bulk flow. The lower part of the vortex head is pushed back slightly, and there is stronger back flow from this head vortex to the entrainment zone of the free jet. After the end of injection, the head of the wall jet is the dominating feature in both scalar and velocity fields. Figure 2 shows that the vortex center, identified here simply by visual inspection of the velocity field, is not in the center of the fuel cloud, but rather downstream of it in the direction of the vortex core's travel. This is because the head vortex is the result of the mean shear between wall jet and the nearly stationary ambient bulk gas, which is being circumferentially entrained by the fuel's momentum.

During the compression stroke, the head of the wall jet moves down the liner, across the piston, and up the liner on the opposite side. In this progression, the differences between low and high tumble increase, as the fuel jet entrains intake-induced momentum. Consistent with conservation of momentum, the difference between the two tumble ratios is about the same as before injection, 0.5 to 1 unit. In a global view, the injection-induced vortex has completely absorbed the intake-induced tumble. The difference in TR between the two cases decreases towards TDC, but this is likely to be due to the relatively smaller portion of the remaining volume that can be imaged.

Increased back flow from jet vortex to free-jet wake for high tumble can be seen very clearly from -110 to -70°CA. The result is that the high-tumble case has a somewhat more homogeneous fuel distribution towards the end of the compression stroke, without the lean pocket on the right that exists for low tumble.

3.2. Turbulence of scalar and velocity

While the evolution of the means show the large-scale convective transport of the fuel and the associated momentum, it is local turbulence that determines mixing of fuel and bulk gas. A detailed analysis of turbulence properties and the associated topic of cycle-to-cycle variation of large-scale structures are beyond the scope of this paper. We restrict the analysis to examination of a couple of single-shot images and the evolution of the root-mean-square (RMS) of scalar and velocity. Only the low-tumble case is examined here. Particular attention is paid to the question of how similarly structured the unsteady wall jet is to a steady free jet.

Figure 4 shows two separate, single-shot (i.e., instantaneous) measurements of fuel mole-fraction and the mean (phase-averaged) in-plane velocity at -85°CA. The scalar images in this figure are thus from different engine cycles. Around the peak mole fraction, the scalar images feature intermittent parcels of high hydrogen concentration with sharp gradients that tend to be at about 45° with respect to the mean velocity field in the more "upstream" portions of the jet head. Two of these structures are marked by the red lines in Figure 4. This 45-degree alignment is also typical of free jets and is thought to correspond to the direction of the maximum mean compressive strain (Ashurst et al. 1987, Vedula et al. 2001). Further "downstream" each of the images shows a large region of high scalar value, whose upstream edge (white line) is closer to 90° with respect to the mean flow. The difference in alignment could be the result of shear between the left cylinder wall and the fuel-rich region between it and the vortex center.

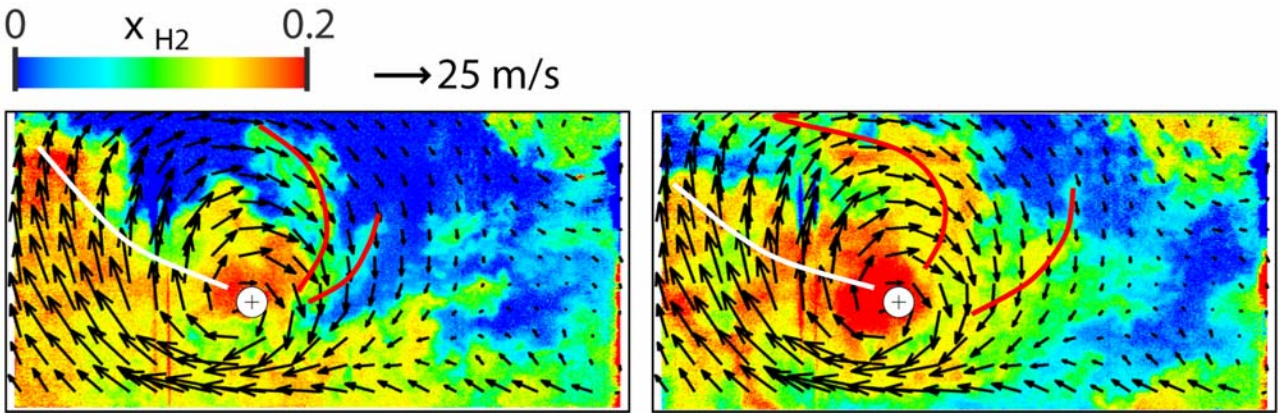

Figure 4 Two single-shot images of *instantaneous* hydrogen mole-fraction (color) and *mean* in-plane velocity (arrows) at -85°CA. Lines indicate large-scale scalar structures; see text.

In canonical turbulent flows, such as steady free jets, the second moments of scalar and velocity are the simplest measures of local turbulence. However, in engines each cycle and each fuel injection brings about a re-initialization of the corresponding flows. The associated large-scale fluctuations are called "cyclic fluctuations", to distinguish the influence of flow re-initialization to the superimposed random fluctuations of the turbulent flow, i.e. the turbulent kinetic energy. Methods such as proper orthogonal decomposition (POD) have been applied to engine flows to approximately differentiate between the two. Here, we will simply discuss the RMS of scalar and velocity without such distinction, keeping in mind that the origin of the fluctuations may be unclear.

Two columns of images in Figure 5 show the RMS of hydrogen mole-fraction (left) and the combined magnitude of the RMS of the two measured in-plane components of the velocity (right). In both columns the large-scale convective structure is indicated by overlaying the mean-velocity vectors. Image pairs from several timings after SOI are shown.

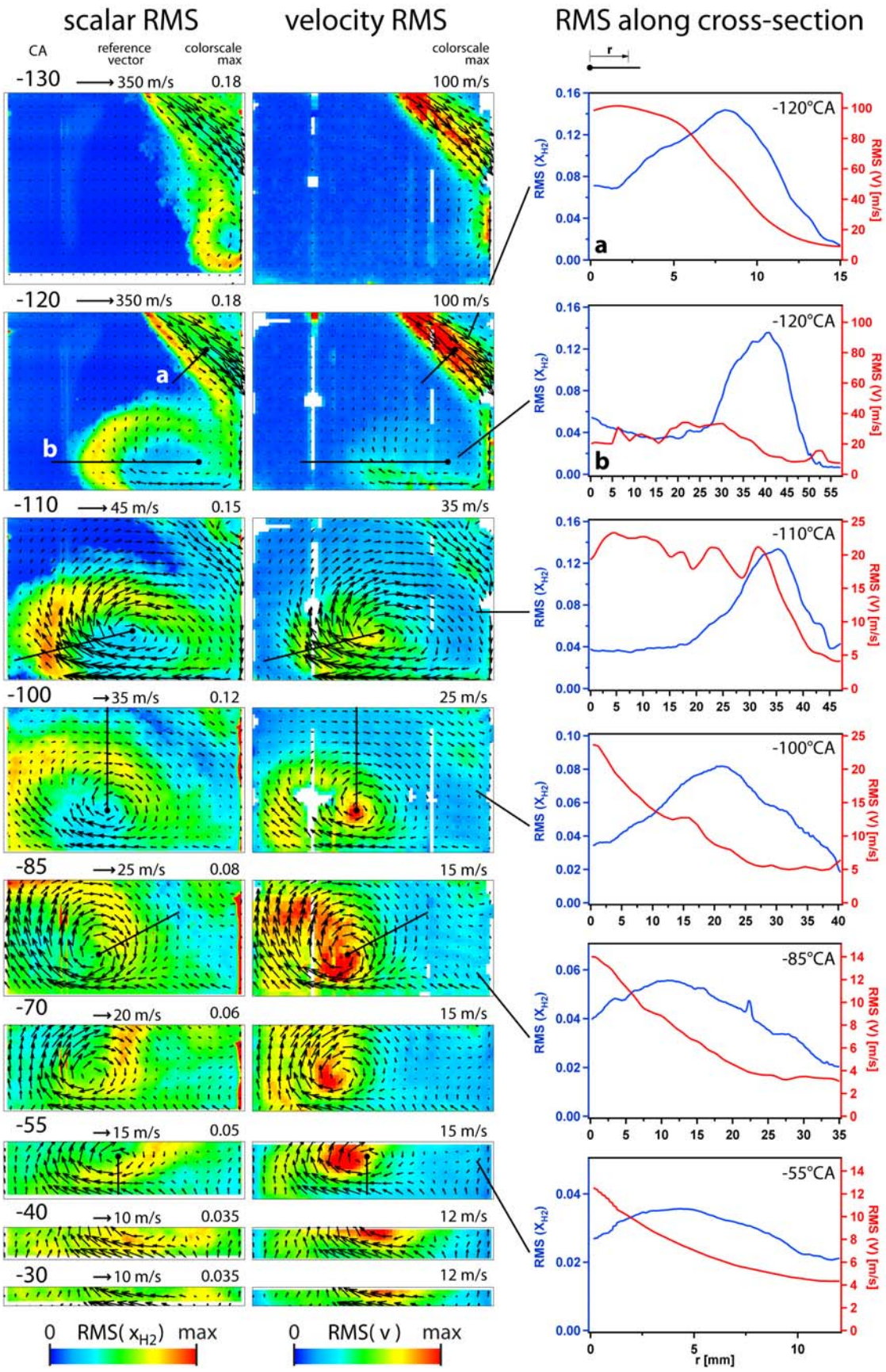

Figure 5 Images: Magnitude of scalar and velocity RMS (background color) and mean velocity (arrows) for low tumble. Above each image pair (left to right): Crank angle, reference vector length, and maxima of color scale for the scalar and velocity RMS. Line plots: Scalar and velocity RMS along the cross-sections indicated in the images at several crank-angles. "a" and "b" label the two different cross-sections at -120ºCA.

At -120 and -130°CA the unimpinged portion of the jet shows reasonable agreement with classic results for subsonic free jets: With about 100 m/s the velocity RMS peaks at about 33% of the peak mean velocity. This is comparable to the results in the far field of air and propane jets (Panchapakesan and Lumley 1993a, Talbot et al. 2009), but is lower than the 46% peak turbulence intensity that has been measured in a helium jet (Panchapakesan and Lumley 1993b)[2]. In fully developed, axisymmetric, turbulent jets the velocity RMS peaks at radial locations on or slightly off the jet axis (Wygnanski and Fiedler 1969, Panchapakesan and Lumley 1993b, Panchapakesan and Lumley 1993a, Talbot et al. 2009), while the scalar RMS peaks well off the jet axis (Becker et al. 1967, Dowling and Dimotakis 1990, Richards and Pitts 1993, Schefer et al. 2008, Talbot et al. 2009). Figure 5 shows that most of the unimpinged jet at -120 and -130°CA is measured to be qualitatively consistent with that.

In fact, this distinct spatial separation between velocity and scalar RMS, with the scalar RMS peaking "around" the region of maximum velocity RMS, persists throughout the compression stroke for as long as the wall-jet head vortex can be distinguished. However, in the wall jet the peak velocity RMS does not spatially coincide with the peak mean velocity. To show this aspect of the developing wall jet more clearly, Figure 5 includes line plots of scalar and velocity RMS along the cross-sections marked in the images, each starting at the approximate vortex center. 40 pixels (7.2 mm) perpendicular to each line were integrated to improve precision. The velocity statistics in the wall jet at -120 and -110°CA suffer from poor data quality due to reflections, but nevertheless a transition between these crank-angles is discernable in which the collocation of vortex core and peak velocity RMS is established. During the remainder of the compression stroke, the profile of the scalar RMS widens relative to the decay in velocity RMS from center to periphery.

4. Conclusions

Results of separate laser-based imaging of hydrogen mole-fraction and in-plane velocity in a motored engine with direct injection of hydrogen during the compression stroke were presented. The fuel jet, issued from an angled single-hole nozzle for about 2 ms just after intake-valve closure, impinges on the liner and forms a wall jet. Entraining the cylinder charge during the compression stroke, the wall jet imparts a tumble-like global rotation onto the charge. The interaction of this jet-induced convection with that remaining from the intake stroke can be observed in detail.

The large-scale convection and mixing pattern is shown by the evolution of mean velocity and scalar field throughout the compression stroke. Two cases are compared: The "standard" intake-port configuration, with a BDC tumble ratio of 0.24 ("low tumble"), and a tumble-enhanced modified version, with a tumble ratio of 0.94 ("high tumble"). Since with the chosen injector targeting injection-induced convection and intake-induced tumble flow counter-act, the high tumble case is in general retarded in the development of its circular convection pattern. Initially, with higher tumble the core of the wall-jet vortex is lifted further from the walls. Consistent with conservation of momentum, the difference in tumble ratio after injection is similar to what it was before injection. Towards the end of the compression stroke, peak mean velocities are higher for the low-tumble case, which reflects the smaller impact of the intake-induced flow on the injected momentum. The final mixture distribution is significantly different between the two cases.

[2] Note that PIV measurements in the portions of the jet that have hydrogen mole-fraction close to unity are likely to be inaccurate. Because the hydrogen fuel contains no seeding particles, valid vectors in the underlying single shots can be obtained only where locally some mixing of fuel and bulk gas has taken place, which in turn also means loss of local momentum due to dilution. Conversely, the instantaneously fastest parts of the jet are often particle-free and not measurable, biasing the mean towards lower values.

In addition to the mean fields, the RMS of velocity and scalar were calculated as a step towards evaluating the turbulence properties of the flows. Upstream of the impingement point, the hydrogen jet behaves much as described by the ample literature on subsonic, fully developed, turbulent, axisymmetric jets: Peak velocity-RMS values of about one-third of the peak mean velocity, radial separation of peak velocity RMS from peak scalar RMS. The latter persists throughout the development of the wall jet. The maximum in velocity RMS for crank angles more than 10 degrees after end the of injection is nearly collocated with the center of the wall-jet vortex. Intermittent scalar structures at the edge of the jet's head show the signature of shear alignment, like those in turbulent free jets.

The data presented here are part of a larger data set, still being expanded, on in-cylinder hydrogen/air mixing in Sandia's optically accessible hydrogen engine. In addition to helping understand the mixture preparation (and eventually the stratified combustion) in hydrogen DI engines, the data are being used for model development. The absence of two-phase flow, soot, or complex chemistry make the hydrogen engine an ideal benchmark for detailed examination of simulation fidelity. In the spirit of furthering simulation development, we intend to publish data from laser-based measurements in the engine on the web as part of the Engine Combustion Network this summer (Picket 2010).

Acknowledgments

The excellent technical support by G. Hux at Sandia is greatly appreciated, as are valuable contributions by Thomas Wallner's group at Argonne National Laboratory. Financial support for this research was provided by the U.S. Department of Energy, Office of Energy Efficiency and Renewable Energy (program manager Gurpreet Singh). The research was performed at the Combustion Research Facility, Sandia National Laboratories, Livermore, California. Sandia is operated by Sandia Corporation, a Lockheed Martin Company, for the United States Department of Energy's National Nuclear Security Administration under contract DE-AC04-94AL85000.

References

Arcoumanis C, Godwin SN, Kim JW (1998) Effect of tumble strength on combustion and exhaust emissions in a single-cylinder, four-valve, spark-ignition engine. SAE Technical Paper 981044

Ashurst WT, Kerstein AR, Kerr RM, Gibson CH (1987) Alignment of vorticity and scalar gradient with strain rate in simulated navier-stokes turbulence. Phys Fluids 30:2343-2353

Becker HA, Hottel HC, Williams GC (1967) Nozzle-fluid concentration field of round turbulent free jet. J Fluid Mech 30:285-303

Boree J, Maurel S, Bazile R (2002) Disruption of a compressed vortex. Phys Fluids 14:2543-2556 DOI 10.1063/1.1472505

Bradley D, Lawes M, Liu K, Verhelst S, Woolley R (2007) Laminar burning velocities of lean hydrogen-air mixtures at pressures up to 1.0 mpa. Combust Flame 149:162-172 DOI 10.1016/j.combustflame.2006.12.002

Delorme A, Rousseau A, Sharer P, Pagerit S, Wallner T (2009) Evolution of hydrogen fueled vehicles compared to conventional vehicles from 2010 to 2045. SAE Technical Paper 2009-01-1008

Dowling DR, Dimotakis PE (1990) Similarity of the concentration field of gas-phase turbulent jets. J Fluid Mech 218:109-141

Edwards R, Mahieu V, Griesemann J-C, Larivé J-F, Rickeard DJ (2004) Well-to-wheels analysis of future automotive fuels and powertrains in the european context. SAE Technical Paper 2004-01-1924

Espey C, Dec JE, Litzinger TA, Santavicca DA (1997) Planar laser rayleigh scattering for quantitative vapor-fuel imaging in a diesel jet. Combust Flame 109:65-86

He Y, Selamet A, Reese RA, Vick RK, Amer AA (2007) Impact of tumble on combustion in si engines: Correlation between flow and engine experiments. SAE Technical Paper 2007-01-4003

Hill PG, Zhang D (1994) The effects of swirl and tumble on combustion in spark-ignition engines. Prog Energy Combust Sci 20:373-429

Hwang W, Dec JE, Sjoberg M (2007) Fuel stratification for low-load hcci combustion: Performance and fuel-plif measurements. SAE Technical Paper 2007-01-4130

Karim GA (2003) Hydrogen as a spark ignition engine fuel. Int J Hydrogen Energy 28:569-577

Keane RD, Adrian RJ (1992) Theory of cross-correlation analysis of piv images. Appl Sci Res 49:191-215

Keane RD, Adrian RJ, Zhang Y (1995) Superresolution particle imaging velocimetry. Meas Sci Technol 6:754-768

Khalighi B (1990) Intake-generated swirl and tumble motions in a four-valve engine with various intake configurations~flow visualization and particle tracking velocimetry. SAE Technical Paper 900059

Knop V, Benkenida A, Jay S, Colin O (2008) Modelling of combustion and nitrogen oxide formation in hydrogen-fuelled internal combustion engines within a 3d cfd code. Int J Hydrogen Energy 33:5083-5097 DOI 10.1016/j.ijhydene.2008.06.027

Li Y, Zhao H, Peng Z, Ladommatos N (2002) Particle image velocimetry measurement of in-cylinder flow in internal combustion engines - experiment and flow structure analysis. Proc Inst Mech Eng Part D-J Automob Eng 216:65-81

Miles PC, Hildingsson L, Hultqvist A (2007) The influence of fuel injection and heat release on bulk flow structures in a direct-injection, swirl-supported diesel engine. Exp Fluids 43:273-283 DOI 10.1007/s00348-007-0281-7

Moreau J, Boree J, Bazile R, Charnay G (2004) Destabilisation of a compressed vortex by a round jet. Exp Fluids 37:856-871 DOI 10.1007/s00348-004-0869-0

Muller SHR, Bohm B, Gleissner M, Grzeszik R, Arndt S, Dreizler A (2010) Flow field measurements in an optically accessible, direct-injection spray-guided internal combustion engine using high-speed piv. Exp Fluids 48:281-290 DOI 10.1007/s00348-009-0742-2

Panchapakesan NR, Lumley JL (1993a) Turbulence measurements in axisymmetrical jets of air and helium .1. Air-jet. J Fluid Mech 246:197-223

Panchapakesan NR, Lumley JL (1993b) Turbulence measurements in axisymmetrical jets of air and helium .2. Helium jet. J Fluid Mech 246:225-247

Picket LM (2010) Engine combustion network. https://share.sandia.gov/ecn/. Accessed 05/12/2010

Richards CD, Pitts WM (1993) Global density effects on the self-preservation behavior of turbulent free jets. J Fluid Mech 254:417-435

Rousseau A, Wallner T, Pagerit S, Lohse-Busch H (2008) Prospects on fuel economy improvements for hydrogen-powered vehicles. SAE Technical Paper 2008-01-2378

Salazar VM, Kaiser SA (2009) An optical study of mixture preparation in a hydrogen-fueled engine with direct injection using different nozzle designs. SAE Technical Paper 2009-01-2682

Salazar VM, Kaiser SA (2010) Influence of the in-cylinder flow field (tumble) on the fuel distribution in a di hydrogen engine using a single-hole injector. SAE Technical Paper 2010-01-0579

Salazar VM, Kaiser SA, Halter F (2009) Optimizing precision and accuracy of quantitative plif of acetone as a tracer for hydrogen fuel. SAE Technical Paper 2009-01-1534

Schefer RW, Houf WG, Williams TC (2008) Investigation of small-scale unintended releases of hydrogen: Momentum-dominated regime. Int J Hydrogen Energy 33:6373-6384 DOI 10.1016/j.ijhydene.2008.05.041

Talbot B, Mazellier N, Renou B, Danaila L, Boukhalfa MA (2009) Time-resolved velocity and concentration measurements in variable-viscosity turbulent jet flow. Exp Fluids 47:769-787 DOI 10.1007/s00348-009-0729-z

Thurber MC, Grisch F, Kirby BJ, Votsmeier M, Hanson RK (1998) Measurements and modeling of acetone laser-induced fluorescence with implications for temperature-imaging diagnostics. Appl Optics 37:4963-4978

Thurber MC, Hanson RK (1999) Pressure and composition dependences of acetone laser-induced fluorescence with excitation at 248, 266, and 308 nm. Appl Phys B - Lasers Opt 69:229-240

Vedula P, Yeung PK, Fox RO (2001) Dynamics of scalar dissipation in isotropic turbulence: A numerical and modelling study. J Fluid Mech 433:29-60

Wallner T, Nande AM, Naber J (2008) Evaluation of injector location and nozzle design in a direct-injection hydrogen research engine. SAE Technical Paper 2008-01-1785

Wallner T, Nande AM, Naber JD (2009) Study of basic injection configurations using a direct-injection hydrogen research engine. SAE Technical Paper 2009-01-1008

Westerweel J (1994) Efficient detection of spurious vectors in particle image velocimetry data. Exp Fluids 16:236-247

White CM, Steeper RR, Lutz AE (2006) The hydrogen-fueled internal combustion engine: A technical review. Int J Hydrogen Energy 31:1292-1305

Wygnanski I, Fiedler H (1969) Some measurements in the self-preserving jet. J Fluid Mech 38:577-612

Yeh C-N, Kamimoto T, Kosaka H, Kobori S (1994) Quantitative measurement of 2-d fuel vapor concentration in a transient spray via a laser-induced fluorescence technique. SAE Technical Paper 941953